24th COBEM - 2017

24th ABCM International Congress of Mechanical Engineering
December 3-8, 2017, Curitiba, PR, Brazil

COBEM-2017-1291
DYNAMICS OF BLOOD FLOW IN CORONARY ARTERY

Hongrui Wang
Sean McGinty
University of Glasgow, Glasgow, United Kingdom
hongruiwang1987@gmail.com, sean.mcginty@glasgow.ac.uk

Rachel M. Lucena
Jose Pontes
Gustavo R. Anjos
Norberto Mangiavacchi
State University of Rio de Janeiro - UERJ, R. Fonseca Teles 524, 20550-013, Rio de Janeiro, Brazil
rachel.lucena@uerj.br, jose.pontes@uerj.br, gustavo.anjos@uerj.br, norberto@uerj.br

Abstract. *The present work aims at developing a computational framework to simulate coronary artery flows in axisymmetric coordinates. An accurate method capable of capturing the flow dynamics is strictly required. In this article an Finite Element Method (FEM) is used to solve the equations governing the motion of the blood flow found in coronary artery as incompressible fluid. An in-house code, previously implemented by Anjos (2012); Anjos et al. (2014), is further developed and presently extended first to better model coronary flows.*

Keywords: *Stents, Coronory Artery, Finite Element Method, hemodynamics*

1. INTRODUCTION

According to the World Health Organisation, in 2010 approximately 17.3 million people, or 30% of all deaths worldwide, died from some form of cardiovascular disease, with coronary artery disease (CAD) accounting for 7.3 million of these deaths. CAD is particularly prevalent in Brazil and the UK. It is estimated that about 30% of deaths occurring in Brazil are from CAD (DATASUL 2003) and this represents a huge economic burden on society. The economic cost is 3.5 billion pounds a year in the UK alone. Ageing populations and increased levels of obesity ensures that CAD will remain a significant public health problem in the future, and is expected to become the leading cause of death worldwide by the year 2020. The development of more effective and low cost treatments for CAD are of great importance for both countries.

The dynamics of blood flow in coronary artery and possible influence of stents struts with computational fluid dynamics (CFD) requires a robust numerical method to compute the solution of the differential equations in a relevant model. We consider the model of dissolution and transport of sirolimus on an axisymmetric domain representing the polymer coating layer and the and the hydrodynamic of the blood flow in the artery in the vicinity of a stent strut as suggested by Bozsak *et al.* (2014) and McGinty and Pontrelli (2016). We employ the Finite Element method on an unstructured mesh for the discretization of the incompressible single-phase Navier-Stokes, the continuity and the energy equation using the Arbitrary Eulerian-Lagrangian framework in axisymmetric coordinate. The blood flow in the arterial wall is considered to be Newtonian. Also, the effect of the releasing process of the polymers is considered. However, the spatial distribution of the sirolimus is greatly influenced by the flow and the arterial wall properties, being therefore susceptible to patient health conditions. The difference of artery shapes and existence of the struts have been investigated in 6 test cases in the influence on the flow dynamics and the transport of a chemical species.

In the following sections of this paper, the mathematical formulation used to model single-phase flows for coronary artery blood flow will be detailed. Several numerical simulations will be presented and focused to validate the implemented FEM algorithm. Finally, conclusions from this study will be discussed.

2. MATHEMATICAL MODELLING AND DISCRETIZATION

The classical description of single-phase flow is based on the governing equations of continuum mechanics of flowing media or hydrodynamics. In the present work, blood flow is a single-phase incompressible fluid modeled by the non-dimensional Navier-Stokes equations written in the Arbitrary Lagrangian-Eulerian description, the continuity equation and the energy equation using axisymmetric coordinates:

$$\frac{D\mathbf{v}}{Dt} = -\nabla p + \frac{1}{Re}\begin{bmatrix} \frac{1}{r}\frac{\partial}{\partial r}r\frac{\partial v}{\partial r} + \frac{\partial^2 v}{\partial r^2} - \frac{2u}{r} \\ \frac{1}{r}\frac{\partial}{\partial r}r\frac{\partial u}{\partial r} + \frac{\partial^2 u}{\partial x^2} \end{bmatrix} \tag{1}$$

$$\frac{\partial u}{\partial x} + \frac{\partial v}{\partial r} + \frac{v}{r} = 0 \tag{2}$$

$$\frac{De}{Dt} = +\frac{1}{ReSc}\left(\frac{1}{r}\frac{\partial}{\partial r}r\frac{\partial e}{\partial r} + \frac{\partial^2 e}{\partial x^2}\right) \tag{3}$$

where $\mathbf{v}$ is the velocity field in axisymmetric coordinates with axial u and radial v components, t represents time, p pressure, r is radial position and e is the scalar field. The non-dimensional numbers Reynodls Re and Sc are defined as:

$$Re = \frac{\rho_0 v_\infty R}{\mu_0}, \qquad Sc = \frac{\mu_0}{\rho_0 \mathcal{D}}$$

note that the above non-dimensional groups are achieved by using the standard parameters when the velocity of the system is known, where v_∞ and R are referential parameters for velocity and channel radius respectively, and $\mathcal{D}$ is mass diffusivity.

The material derivative $D\mathbf{v}/Dt$ describes the rate of change of the velocity with time, and in the moving mesh context, it turns into a partial ordinary derivative, thus the convective term vanishes while the coordinates are instantaneously changed.

$$\frac{D\mathbf{v}}{Dt} = \frac{\partial \mathbf{v}}{\partial t} + \mathbf{c}\cdot\nabla\mathbf{v} \tag{4}$$

where $\mathbf{c} = \mathbf{v} - \hat{\mathbf{v}}$ is an arbitrary velocity given by the difference between the fluid velocity $\mathbf{v}$ and the mesh velocity $\hat{\mathbf{v}}$. The fully Lagrangian description of the fluid motion can be achived by setting $\hat{\mathbf{v}} = \mathbf{v}$ where the fully Eulerian description can be easily achieved where $\hat{\mathbf{v}} = 0$. In the ALE context, an arbitrary value may be selected depending upon the simulation and the behavior of the flow field itself. An scheme is here proposed to find the suitable value for the mesh velocity $\hat{\mathbf{v}}$ at the postion $\mathbf{x}$ as follows:

$$\hat{\mathbf{v}}(\mathbf{x}) = \beta_1\mathbf{v} + \beta_2\mathbf{v}_e \tag{5}$$

where β_1 and β_2 are parameters which varies from 0 to 1 and $\mathbf{v}_e$ is an elastic velocity based on the Laplacian Smooth operator as described in details in Anjos (2012). The appropriate choice of these parameters lead to a well distribuited mesh with high quality triangular elements. The material derivative can be discretized using the Semi-Lagrangian method as described in Anjos (2007) and Anjos (2012):

$$\frac{D\mathbf{v}}{Dt} = \frac{\mathbf{v}^{n+1}(\mathbf{x}^n) - \mathbf{v}^n(\mathbf{x}_d^{n-1})}{\Delta t} \tag{6}$$

where $\mathbf{v}^n(\mathbf{x}_d^{n-1}) = \mathbf{v}^n(x_d, t^n)$ and x_d is the departure point. In the strong form, the substantial derivative is calculated along the characteristic trajectory, thus finding the point x_d by solving $D\mathbf{v}/Dt = f$ backwards in time $t^{n+1} \geq t \geq t^n$ using the initial condition $x(t^{n+1}) = x_i$. The initial position x_i in time t^{n+1} is known and therefore it is used to find the departure point x_d, whose position is unknown. The same method is successfuly applied to discretize the material derivative of the energy equation De/Dt. The gradient in axisymmetric formulation read as $\nabla\bullet = (\partial\bullet/\partial x, \partial\bullet/\partial r)^T$.

Boundary conditions are required to find the particular solution of the partial differential equations presented above for the solution of the two-phase flow system. Since the geometry and the flow variables are assumed to be independent of the rotation angle θ, a symmetry boundary condition of

$$v = 0 \qquad \text{and} \qquad \frac{\partial u}{\partial r} = 0 \tag{7}$$

is required on the symmetry axis ($r = 0$). The present model assumes no-slip condition on the artery wall and symmetric condition on the symmetric axis. For all test cases presented here, the symmetric axis is set to $r = 0$. Flow at inlet of the channel is assumed to have parabolic velocity profile in axisymmetric coordinates. Pressure at outlet is the reference pressure and a concentration field is set to the its saturation where the stent geometry holds.

The discretization of the numerical domain is achieved by a collection of triangles interconnected where the interface between fluids is the triangle edge of the own generated mesh. The *mini*-element is used to compute pressure at the triangle vertices and velocity at the triangle vertices and an extra node at the centroid. Velocity and pressure are uncoupled from the resulting linear system through the projection method based on LU decompostion. The final linear systems are solved using direct solver. A block diagram of the described procedure to compute velocity, pressure and concentration fields can be seen in Fig 1.

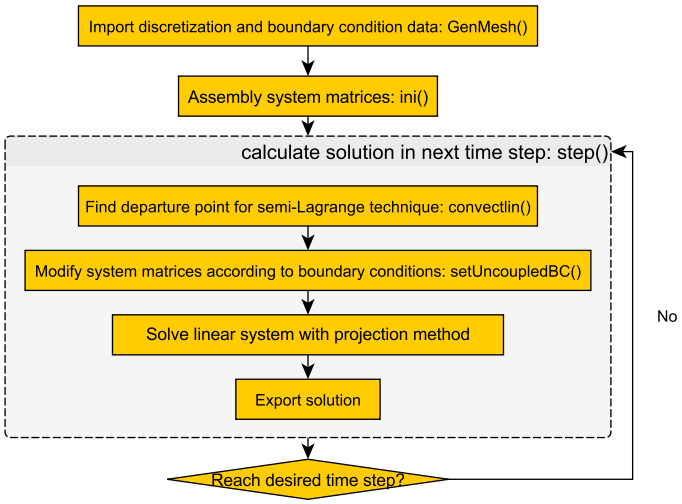

Figure 1. Block diagram of the computational procedure to compute velocity, pressure and concentration fields for the hydrodynamics of blood flow in coronary artery channels.

3. RESULTS

Numerical results are given for several cases of blood flows in artery. The lumen radius of a typical artery is about $R = 1.5$mm, viscosity in the lumen is set to $\mu = 0.0035$Pa.s. and density $\rho = 1060$kg/m^3 as suggested by Bozsak *et al.* (2014). A typical velocity in artery flow is found to be $v = 12$cm/s according to Kessler *et al.* (1998), therefore the Reynolds number is chosen to be $Re = 54.5$ based on the channel radius R as referential length. We adopt a value of the Schmidt number $Sc = 200$ as a starting point to the investigation of the transport of a chemical species for the present work. Several geometries have been used in the simulations as shown in Figs 2a-2f. Aditionally, a chemical species boundary condition was set to maximum concentration $e = 1$ to the top of each numerical domain without the presence of stents. On the other hand, the chemical species e was set to 1 at the strut boundary for the others test cases with the presence of the stents.

The dimensions in x-direction of all geometries are bounded to $[0, 10R]$, where R is the channel radius. The radius of the channel can vary according to the geometries presented. In Fig. 2a the artery channel is modeled as a cylinder channel which walls are straight. The stent geometry is placed on the top of the domain in the cylinder channel as shown in Fig. 2b. In Figs. 2c-2d, the channel is modeled by a smooth constriction at the middle of the channel as found in Venturi channels. A real artery channel is presented in Figs. 2c-2d without and with the insertion of stents respectively. These geometries were obtained by image processing from a coronary artery photography.

3.1 Straight Channel: Hagen-Poiseuille Flow

For the case of idealised geometry with straight artery wall with parabolic velocity inflow, there exist a known analytical solution, which has a parabolic velocity profile for every vertical slice of the tube. In this subsection, we present results for the simulation of the Hagen-Poiseuille flow. The results are then compared to the analytical solution of the velocity profile in axisymmetric coordinate given by:

$$v(x) = 2\left(1 - \frac{r^2}{R^2}\right) \tag{8}$$

where μ represents the dynamic viscosity, p is pressure, R is the channel radius and r is the distance from the axis of symmetry. The inflow and outflow conditions are applied at the left and right boundaries respectively, while the no-slip conditions are set to the remaining boundaries. A domain of $10R \times R$ has been used. The parameters for the mesh velocity was set to $\beta_1 = 0$ and $\beta_2 = 1.0$.

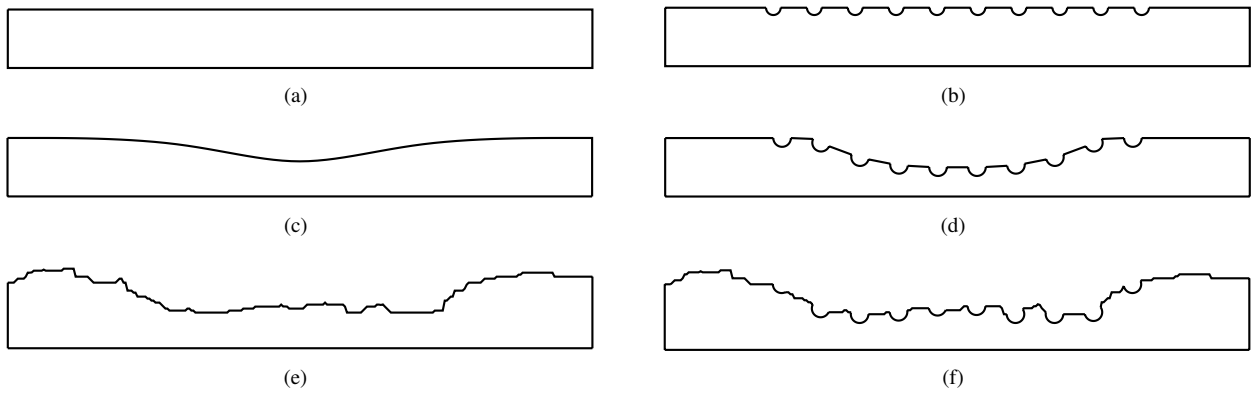

Figure 2. Non-dimensional geometry models for blood flow dynamics in coronary arteries. The channel length $L = 10R$ is based on the channel width $R = 1$. (a) Straight Channel, (b) Straight Channel with Stents, (c) Curved Channel, (d) Curved Channel with Stents, (e) Real Channel and (f) Real Channel with Stents.

Figure 3 shows the transient velocity profile along the radial direction r of the straight channel taken at the middle of the channel length $x = 5.0R$. As can be seen, the time evolution of the velocity profile for non-dimensional time $t = 0.0$ to $t = 6.0$ converges to the analytical solution of the Hagen-Poiseuille flow shown by the continuous line. The numerical solution matches its analytical solution for the mesh proposed in this work, where the total number of elements and mesh nodes (centroid not counted) was 17456 and 9280 respectively.

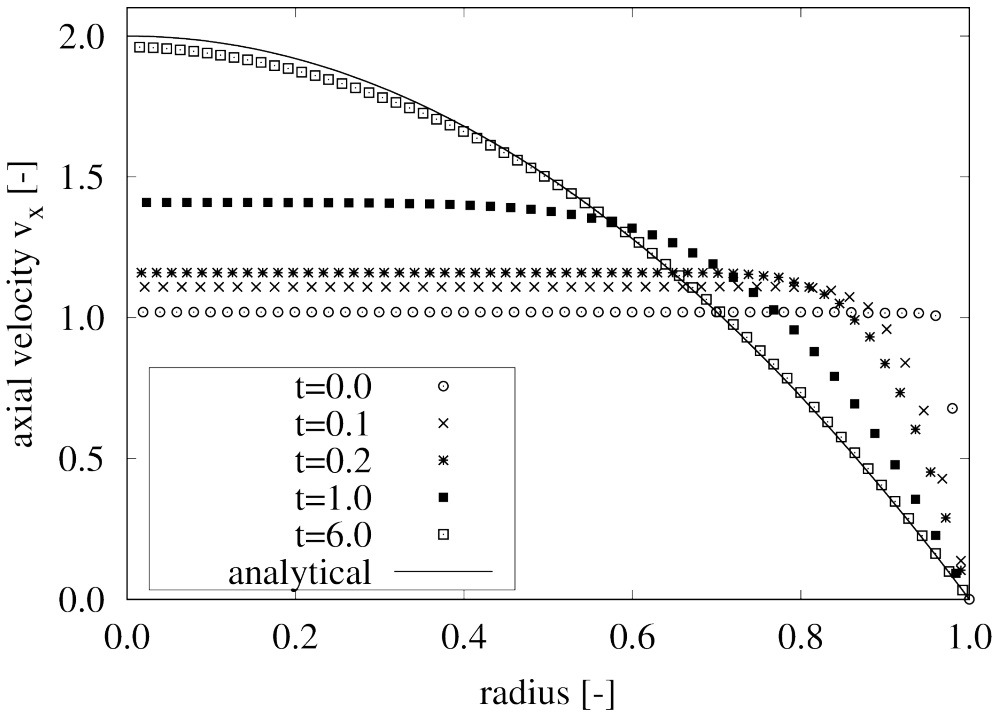

Figure 3. Transient velocity profile for the simulation of the Hagen-Poiseuille flow in an axisymmetric channel which data was taken using interpolation in r-direction at $x = 5.0R$ (half channel length). Velocity v_x, radius r and time t are non-dimensional.

Figure 4 shows the evolution in space and time of the velocity field on the left hand side, Figs. 4a,c,e,g and the chemical species transport on the right hand side, Figs. 4b,d,f,h. The velocity profile at the middle of the channel can be seen quantitatively in Fig. 3. The chemical species field is represented non-dimensionally by the red color indicating maximum value of 1 and blue color indicating minimum value of 0.

3.2 Straight Channel with Stents

In this test case, the stent strut was placed at the top of the domain $r = R$ and it is modeled by 10 semi-circles uniformely spaced. It is worth noting here that such a proposed model is an approximation of the real stent strut found

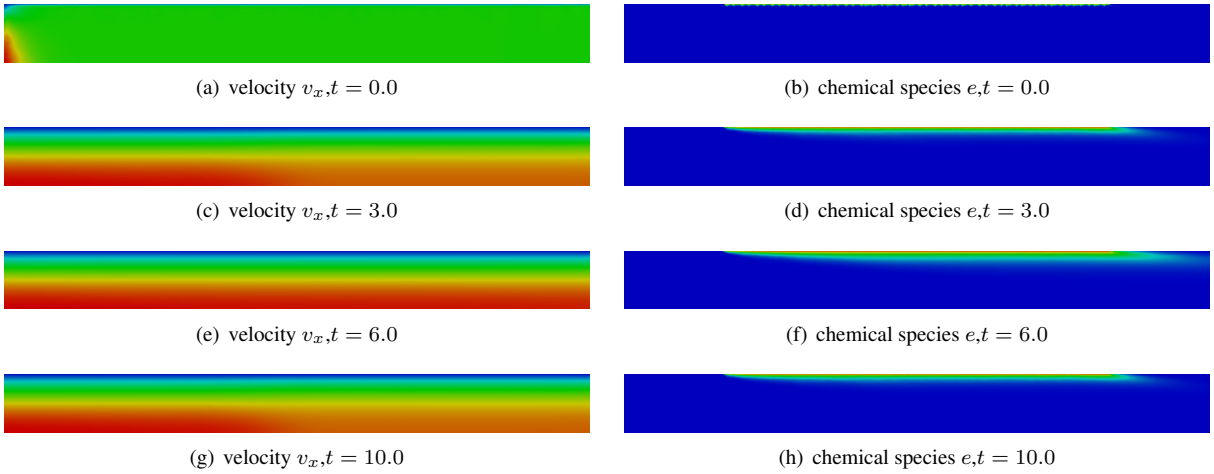

(a) velocity v_x,$t = 0.0$ (b) chemical species e,$t = 0.0$

(c) velocity v_x,$t = 3.0$ (d) chemical species e,$t = 3.0$

(e) velocity v_x,$t = 6.0$ (f) chemical species e,$t = 6.0$

(g) velocity v_x,$t = 10.0$ (h) chemical species e,$t = 10.0$

Figure 4. Time evolution of the velocity (left) and chemical species (right) fields for the straight walls channel. The velocity profile at the middle of the channel can be seen quantitatively in Fig. 3.

in coronary arteries. In fact, many manufactures have proposed different stent geometries as found in Siewiorek *et al.* (2009) and Cosentinoa *et al.* (2014), however a complete representation of the stent geometry is only achieved by a fully 3D solver, which is not the scope of the present paper. The velocity inlet is set to the parabolic profile found as solution of the Hagen-Poiseuille flow in straight channels (see 8).

Figure 5 shows the transient velocity profile along the radial direction r of the straight channel with stents taken at the middle of the channel length $x = 5.0R$. As can be seen, the time evolution of the velocity profile for non-dimensional time $t = 0.0$ to $t = 6.0$ reaches maximum axial velocity of approximately $v_x = 2.3$ at the middle of the channel $r = 0$. The insertion of the stent strut decrease the diameter of the channel, therefore the velocity field is higher at the middle of the channel if compared to the same test case without the presence of the strut. The total number of elements and mesh nodes (centroid not counted) was 17181 and 9182 respectively.

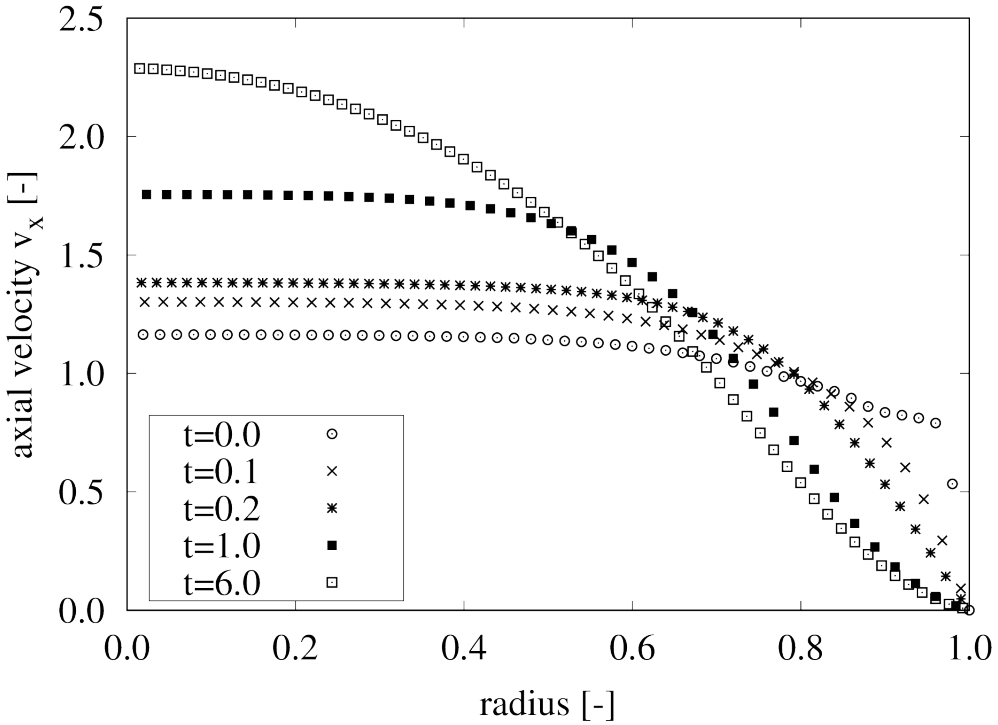

Figure 5. Transient velocity profile for the simulation of the straight channel with stents in an axisymmetric channel which data was taken using interpolation in r-direction at $x = 5.0R$ (half channel length). Velocity v_x, radius r and time t are non-dimensional.

Figure 6 shows the evolution in space and time of the velocity field on the left hand side, Figs. 6a,c,e,g and the chemical species transport on the right hand side, Figs. 6b,d,f,h. The velocity profile at the middle of the channel can

be seen quantitatively in Fig. 5. The chemical species field is represented non-dimensionally by the red color indicating maximum value of 1 and blue color indicating minimum value of 0. As can be seen for the velocity field, an increase of speed is noted between $x = 2.0R$ to $x = 8.0R$, while the chemical species boundary layer does not differs much from the case without the struts.

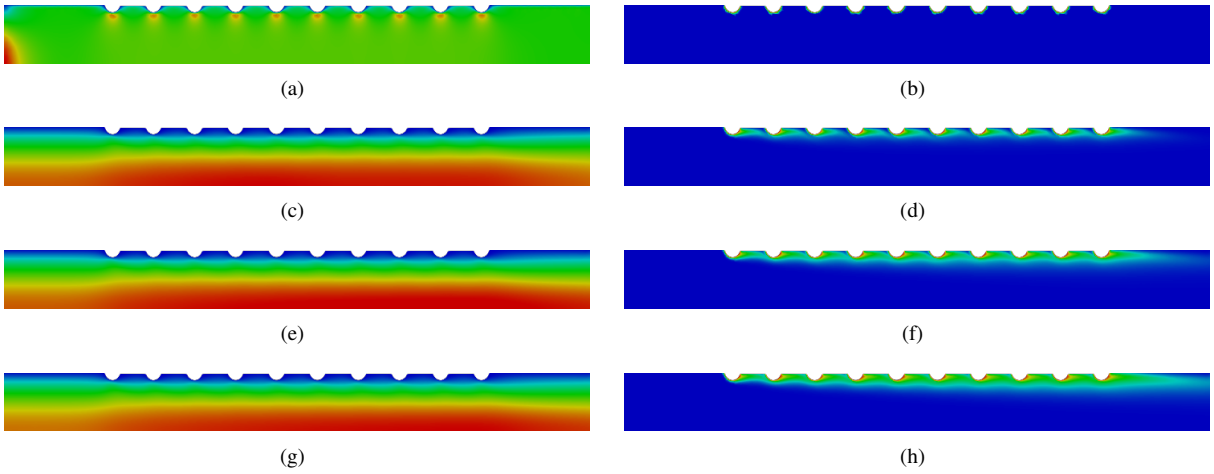

Figure 6. Time evolution of the velocity (left) and chemical species (right) fields for the straight walls channel with stents placed on the top of the domain where $r = max$. The velocity profile at the middle of the channel can be seen quantitatively in Fig. 5.

3.3 Curved Channel

A curved geometry model is proposed in this section and it can be found at Fig. 2c. This geometry promotes a smooth reduction of the channel diameter followed by a smooth expansion as commonly found in Venturi channels as an idealization of the real coronary artery channel. The velocity inlet is set to the parabolic profile found as solution of the Hagen-Poiseuille flow in straight channels (see 8), while the no-slip condition was set to the curved boundary. At the bottom, a symmetry boundary condition was imposed as related to axisymmetric type of flow. An outflow was set at the very end of the channel ($x = 10.0R$) to described reference pressure equal to zero.

Figure 7 shows the transient velocity profile along the radial direction r of the curved channel taken at the middle of the channel length $x = 5.0R$. As can be seen, the time evolution of the velocity profile for non-dimensional time $t = 0.0$ to $t = 1.0$ is smoothly carried out to its steady shape after $t = 1.0$, reaching non-dimensional axial velocity $v_x \approx 4.0$. The total number of elements and mesh nodes (centroid not counted) was 17456 and 9280 respectively.

Figure 8 shows the evolution in space and time of the velocity field on the left hand side, Figs. 8a,c,e,g and the chemical species transport on the right hand side, Figs. 8b,d,f,h. The velocity profile at the middle of the channel can be seen quantitatively in Fig. 7. The chemical species field is represented non-dimensionally by the red color indicating maximum value of 1 and blue color indicating minimum value of 0 and it is located at the convergence and divergence of the channel's geometry. Such a geometry promotes an accumulation of the chemical species after the bump, while its is suppressed at the beginning of the curve.

3.4 Curved Channel with Stents

In this test case, the stent strut was placed at the top of the domain $r = R$ and it is modeled by 10 semi-circles uniformely spaced. It is worth noting here that such a proposed model is an approximation of the real stent strut found in coronary arteries. The velocity inlet is set to the parabolic profile found as solution of the Hagen-Poiseuille flow in straight channels (see 8). The no-slip condition was set to the curved boundary. At the bottom, a symmetry boundary condition was imposed as related to axisymmetric type of flow. The outflow condition was set at the very end of the channel ($x = 10.0R$) to described reference pressure equal to zero.

Figure 9 shows the transient velocity profile along the radial direction r of the curved channel with stents taken at the middle of the channel length $x = 5.0R$. The time evolution of the velocity profile for non-dimensional time $t = 0.0$ to $t = 1.0$ reaches maximum non-dimensional axial velocity of approximately $v_x = 4.0$ at the middle of the channel $r = 0$. As before, the insertion of the stent strut decrease the diameter of the channel, therefore the velocity field is higher at the middle of the channel if compared to the same test case without the presence of the strut. The total number of elements and mesh nodes (centroid not counted) was 12612 and 6717 respectively.

Figure 10 shows the evolution in space and time of the velocity field on the left hand side, Figs. 10a,c,e,g and the

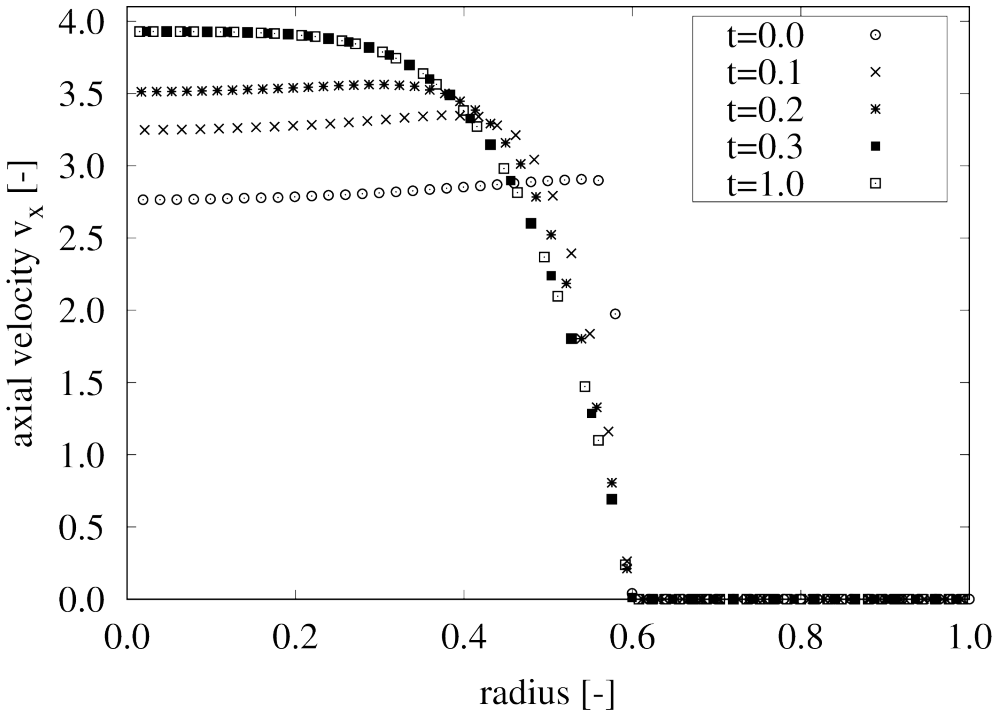

Figure 7. Transient velocity profile for the simulation of the curved channel flow in an axisymmetric channel which data was taken using interpolation in r-direction at $x = 5.0R$ (half channel length). Velocity v_x, radius r and time t are non-dimensional.

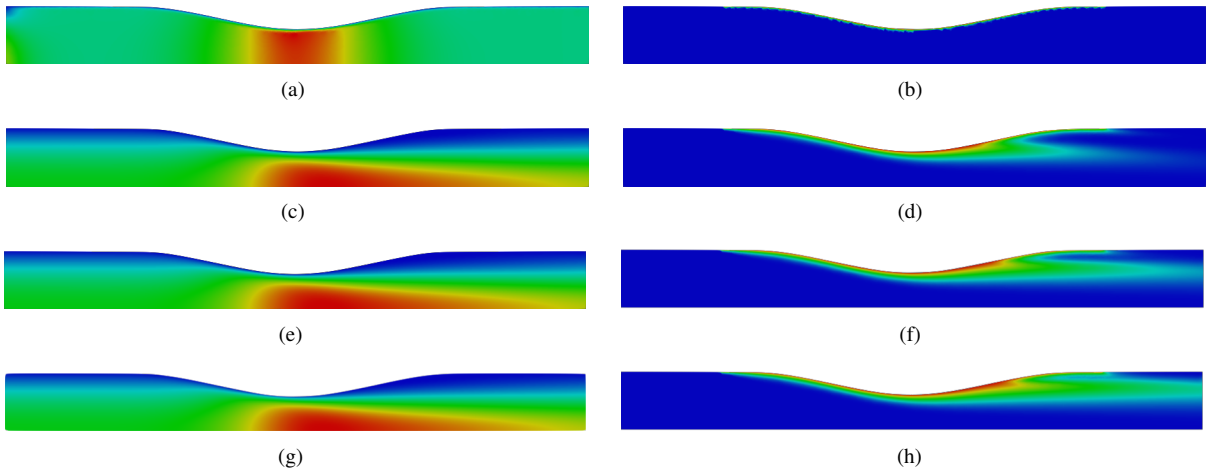

Figure 8. Time evolution of the velocity (left) and chemical species (right) fields for the curved walls channel. The velocity profile at the middle of the channel can be seen quantitatively in Fig. 7.

chemical species transport on the right hand side, Figs. 10b,d,f,h. The velocity profile at the middle of the channel can be seen quantitatively in Fig. 9. The chemical species field is represented non-dimensionally by the red color indicating maximum value of 1 and blue color indicating minimum value of 0. As can be seen for the velocity field, an increase of speed is mainly noted after channel constriction at $x \approx 4.5R$, while the chemical species boundary layer is thicker at the expansion section at $x \approx 7.0R$.

3.5 Real Channel

We performed a numerical simulation of a real artery channel which geometry was taken using image processing from a real coronary artery photography. In the current simulation, the investigation of flow dynamics and transport of the chemical species has been analyzed without the presence of the stent. The parameter used in this simulation are the same parameters as presented in the previous test cases. As can be seen in Fig.2e, the geometry of the channel differs from the geometric models tested in the present work. It is important to note that such a coronary artery geometry is particular to

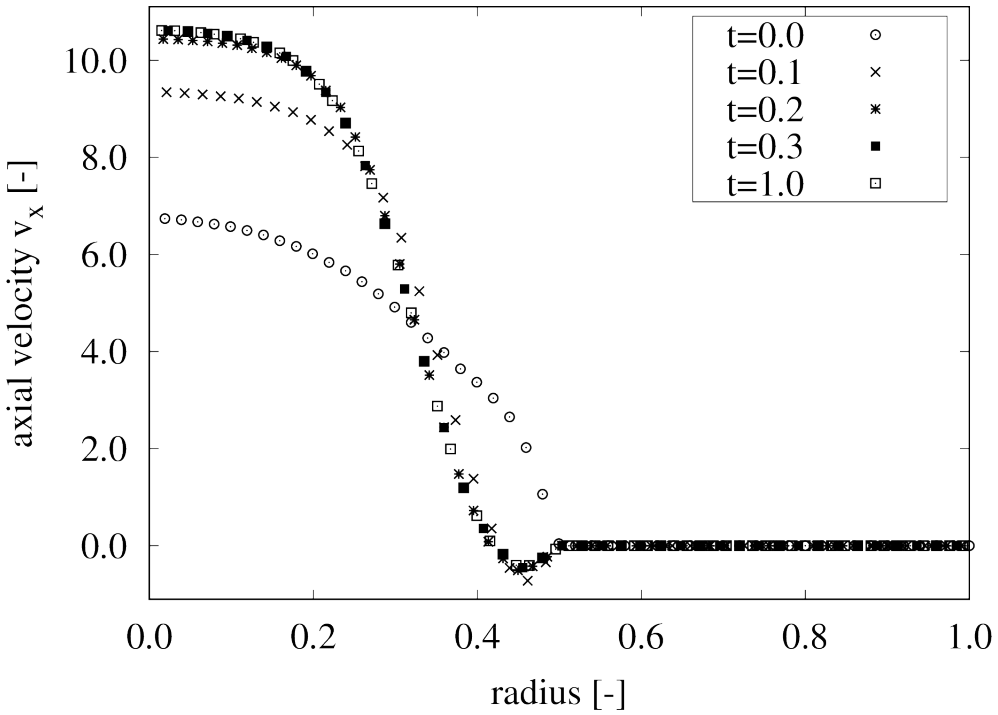

Figure 9. Transient velocity profile for the simulation of the curved channel with stents in an axisymmetric channel which data was taken using interpolation in r-direction at $x = 5.0R$ (half channel length). Velocity v_x, radius r and time t are non-dimensional.

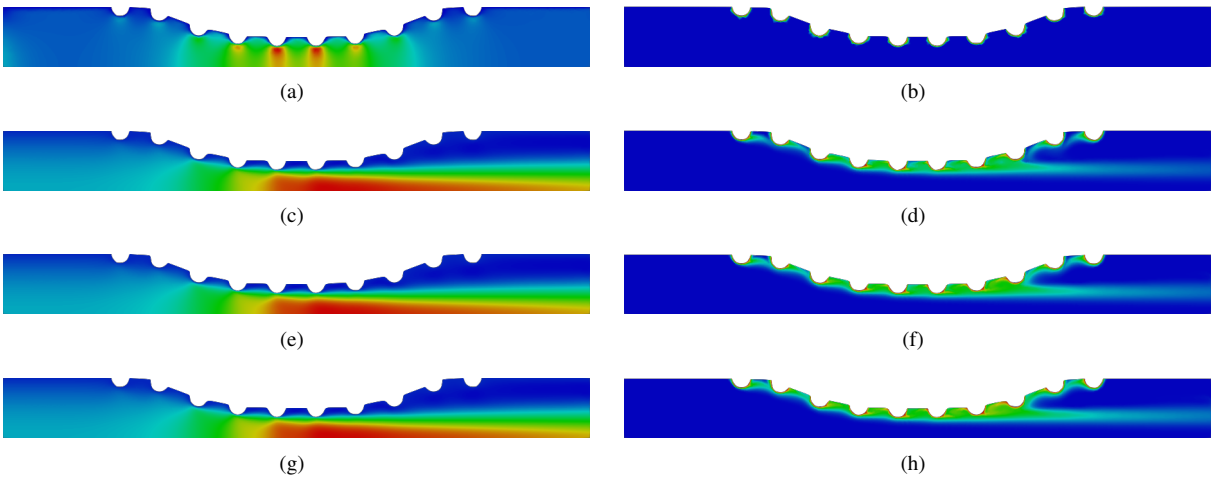

Figure 10. Time evolution of the velocity (left) and chemical species (right) fields for the curved walls channel with the presence of the stent strut. The velocity profile at the middle of the channel can be seen quantitatively in Fig. 9.

each patient and compatible to its health conditions. The velocity inlet is set to the parabolic profile found as solution of the Hagen-Poiseuille flow in straight channels (see 8). The no-slip condition was set to the curved boundary. At the bottom, a symmetry boundary condition was imposed as related to axisymmetric type of flow. Additionaly, an outflow was set at the very end of the channel ($x = 10.0R$) to described reference pressure equal to zero.

Figure 11 shows the transient velocity profile along the radial direction r of the curved channel taken at the middle of the channel length $x = 5.0R$. As can be seen, the time evolution of the velocity profile for non-dimensional time $t = 0.0$ to $t = 1.0$ is smoothly carried out to its steady shape after $t = 1.0$, reaching non-dimensional axial velocity $v_x \approx 6.0$. The total number of elements and mesh nodes (centroid not counted) was 17637 and 9464 respectively.

Figure 12 shows the evolution in space and time of the velocity field on the left hand side, Figs. 12a,c,e,g and the chemical species transport on the right hand side, Figs. 12b,d,f,h. The velocity profile at the middle of the channel can be seen quantitatively in Fig. 11. The chemical species field is represented non-dimensionally by the red color indicating maximum value of 1 and blue color indicating minimum value of 0 and it is located at the constriction of the channel's geometry. Such an irregular geometry promotes inverse axial velocity after the insertion of the stent struts, leading to a

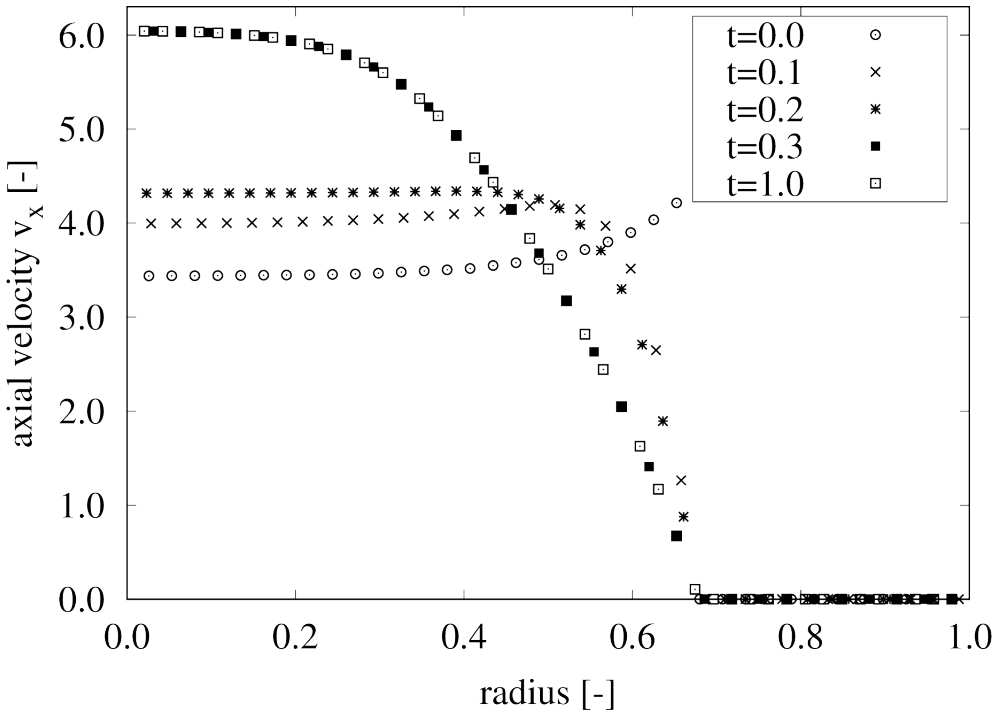

Figure 11. Transient velocity profile for the simulation of the real coronary artery channel flow in an axisymmetric channel which data was taken using interpolation in r-direction at $x = 5.0R$ (half channel length). Velocity v_x, radius r and time t are non-dimensional.

low pressure region.

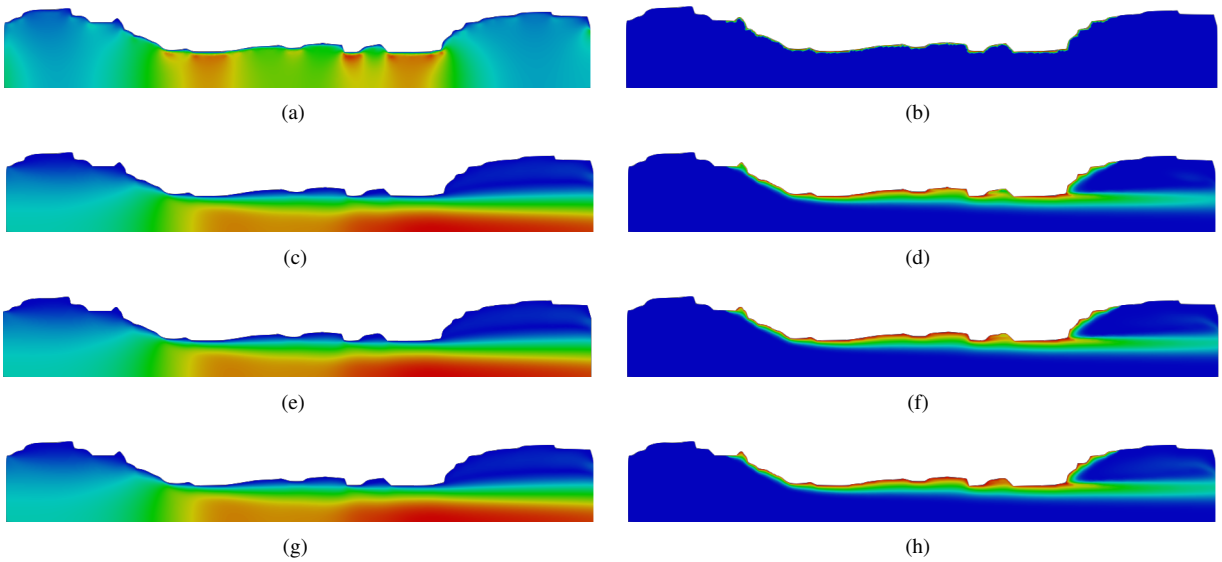

Figure 12. Time evolution of the velocity (left) and chemical species (right) fields for the real artery channel where the shape was taken through image processing. The velocity profile at the middle of the channel can be seen quantitatively in Fig. 11.

3.6 Real Channel with Stents

We present results when the stent strut was placed at the top of the domain $r = R$ and modeled by 10 semi-circles uniformely spaced and distribuited along the boundary contour. The velocity inlet is set to the parabolic profile found as solution of the Hagen-Poiseuille flow in straight channels (see 8). The no-slip condition was set to the curved boundary. At the bottom, a symmetry boundary condition was imposed as related to axisymmetric type of flow. Moreover, an outflow was set at the very end of the channel ($x = 10.0R$) to described reference pressure equal to zero.

Figure 13 shows the transient velocity profile along the radial direction r of the real coronary artery channel with stents taken at the middle of the channel length $x = 5.0R$. The time evolution of the velocity profile for non-dimensional time $t = 0.0$ to $t = 1.0$ reaches maximum non-dimensional axial velocity of approximately $v_x = 9.0$ at the middle of the channel $r = 0$. As before, the insertion of the stent strut decrease the diameter of the channel, therefore the velocity field is higher at the middle of the channel if compared to the same test case without the presence of the strut. The total number of elements and mesh nodes (centroid not counted) was 16894 and 9101 respectively.

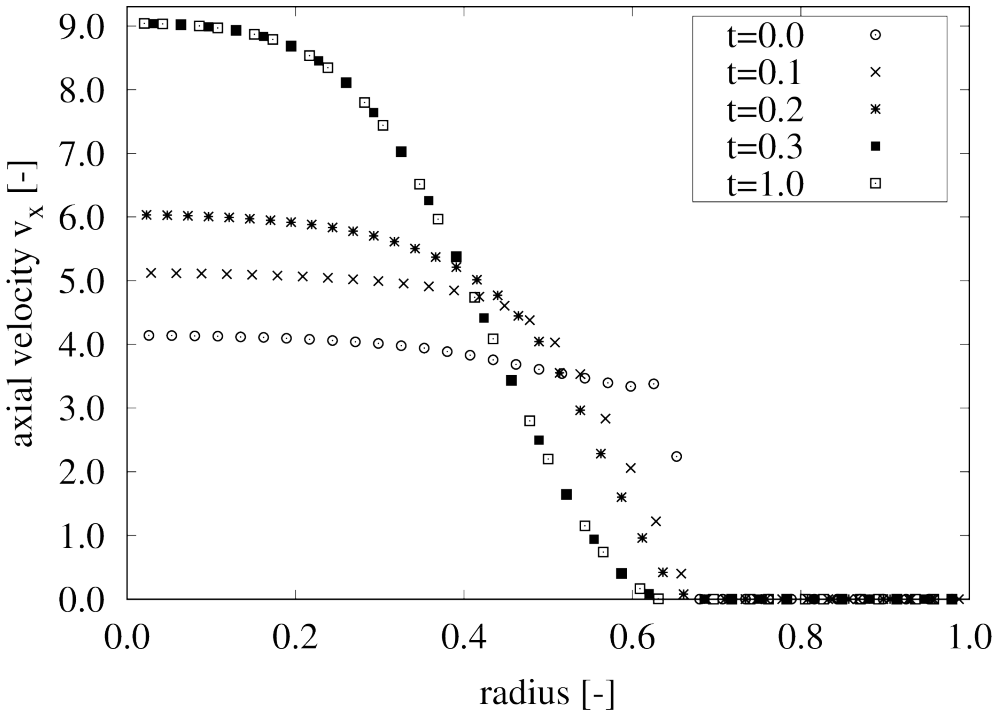

Figure 13. Transient velocity profile for the simulation of the real coronary artery channel with stents in an axisymmetric channel which data was taken using interpolation in r-direction at $x = 5.0R$ (half channel length). Velocity v_x, radius r and time t are non-dimensional.

Figure 14 shows the evolution in space and time of the velocity field on the left hand side, Figs. 14a,c,e,g and the chemical species transport on the right hand side, Figs. 14b,d,f,h. The velocity profile at the middle of the channel can be seen quantitatively in Fig. 13. The chemical species field is represented non-dimensionally by the red color indicating maximum value of 1 and blue color indicating minimum value of 0. As can be seen for the velocity field, an increase of speed is mainly noted after channel constriction at $x \approx 3.0R$, while the chemical species boundary layer assumes an irregular distribuition.

4. CONCLUSIONS

In this article, a moving mesh interface tracking method was presented for the simulation of axisymmetric single-phase flows to investigate the hydrodynamic of blood flow found in coronary artery with deposition of fat at the walls and the insertion of stent struts to release the restriction caused at the artery channel cross section. The method proposed here successfully discretizes the incompressible Navier-Stokes equations with the Finite Element method on an unstructured triangular meshes in complex geometries. Validation of the method was presented for single-phase flow problems including the well-knonw Hagen-Poiseuille flow, showing that the proposed methodology is accurate to represent Newtonian single-phase flows. Several test cases were presented including artery channels with stent struts. Two simulations were performed using an image processing technique to extract the geometry shape of an real coronary artery photography. Additionaly, it has been anaylized that the curved geometry produces similar results of velocity, pressure and concentration field as compared to the real geometry, therefore it may be used to analyze blood flows in artery as a simpler model. We conclude that the proposed methodology is suitable to study in details such a condition in very complex geometries. Further investigations will include chemical species releasing models and flows with presence of more than one phase.

5. ACKNOWLEDGEMENTS

The authors would like to thank CNPq and FAPERJ (Research Support Foundation of the State of Rio de Janeiro) for its support.

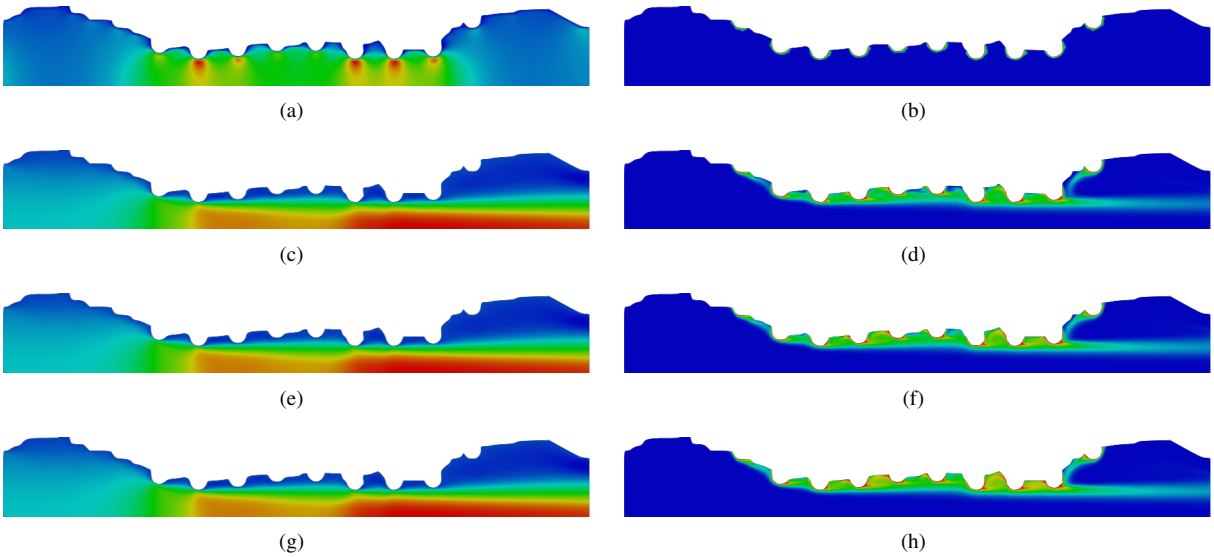

Figure 14. Time evolution of the velocity (left) and chemical species (right) fields for the real artery channel with stents where the shape was taken through image processing. The velocity profile at the middle of the channel can be seen quantitatively in Fig. 13.

6. REFERENCES

Anjos, G., 2007. *Hydrodynamics Field Solution of electrochemical Cells Through Finite Element Method*. Master's thesis, Metallurgical and Materials Engineering, Federal University of Rio de Janeiro, Brazil.

Anjos, G., 2012. *A 3D ALE Finite Element Method for Two-Phase Flows with Phase Change*. Ph.D. thesis, École Polytechnique Fédérale de Lausanne.

Bozsak, F., J-M., C. and Barakat, A., 2014. "Modeling the transport of drugs eluted from stents: physical phenomena driving drug distribution in the arterial wall". *Biomech Model Mechanobiol*, Vol. 13, pp. 327–347. doi:10.1007/s10237-013-0546-4.

Cosentinoa, D., Zwierzak, I., Schievanob, S., DiÌĄaz-Zuccarinia, V., Fenner, J. and Narracott, A., 2014. "Uncertainty assessment of imaging techniques for the 3d reconstruction of stent geometry". *Medical Engineering & Physics*, Vol. 1, pp. 1–7.

Kessler, W., Moshage, W., Galland, A., Zink, D., Achenbach, S., Nitz, W., Laub, G. and Bachmann, K., 1998. "Assessment of coronary blood flow in humans using phase difference mr imaging comparison with intracoronary doppler flow measurement". *International Journal of Cardiac Imaging*, Vol. 14, pp. 179–186.

McGinty, S. and Pontrelli, G., 2016. "On the role of specific drug binding in modelling arterial eluting stents". *Journal of Mathematical Chemistry*, Vol. 54, pp. 967–976.

Siewiorek, G.M., Finol, E.A. and Wholey, M.H., 2009. "Clinical significance and technical assessment of stent cell geometry in carotid artery stenting". *Endovascular Therapy Reviews*, Vol. 16, pp. 178–188.

7. RESPONSIBILITY NOTICE

The authors are the only responsible for the printed material included in this paper.